Radiative Transfer Modeling of Surface Chemical Deposits

Paper 9840-21 presented at SPIE DCS 2016

Thomas A. Reichardt and Thomas J. Kulp
**Sandia National Laboratories**
**P. O. Box 969, MS 9033, Livermore, CA 94551**

April 19th, 2016

Silica Powders: A Visible Example of Morphological Dependence
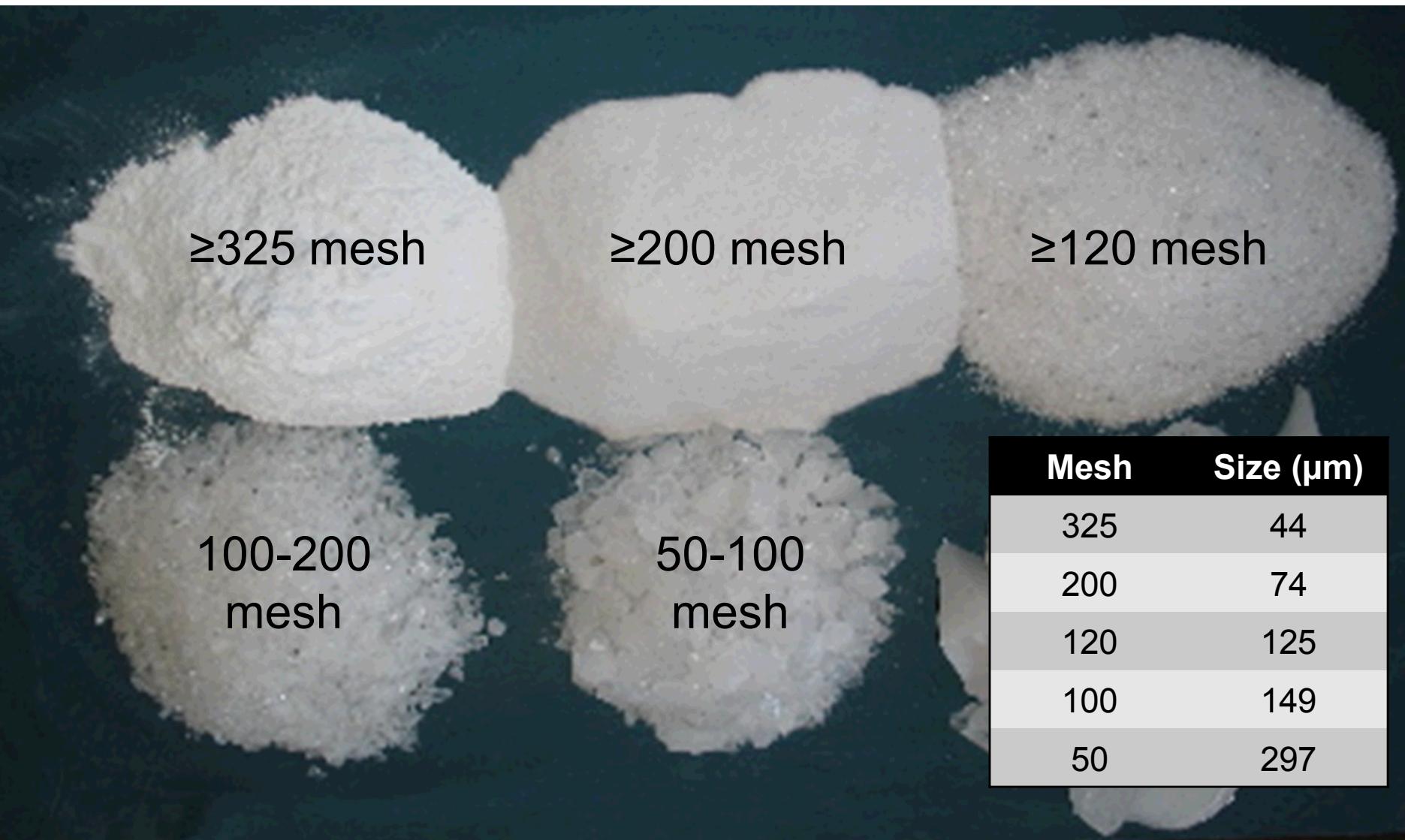
≥325 mesh

≥200 mesh

≥120 mesh

100-200 mesh

50-100 mesh

Mesh	Size (µm)
325	44
200	74
120	125
100	149
50	297

Sandia National Laboratories

Silica Powers: An Infrared Example of the Morphological Dependence (as presented earlier today by Kulp et al. in *Paper 9840-16*)
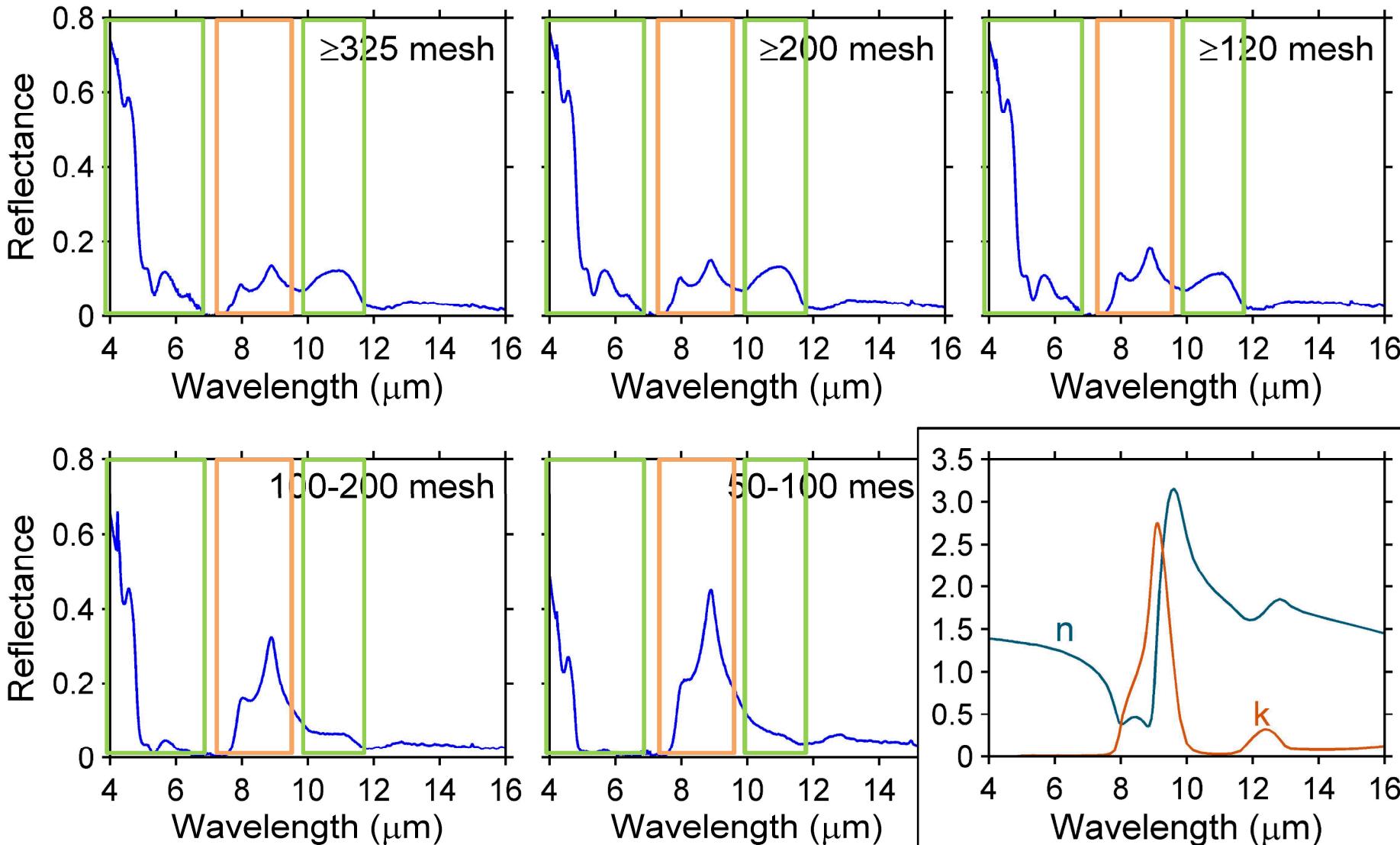
Silica Powers: An Infrared Example of the Morphological Dependence (as presented earlier today by Kulp et al. in *Paper 9840-16*)
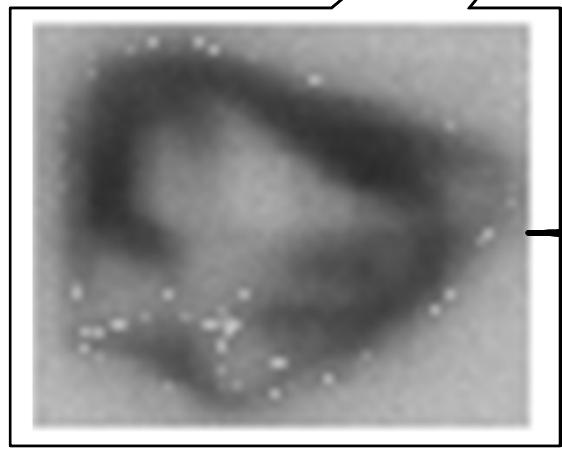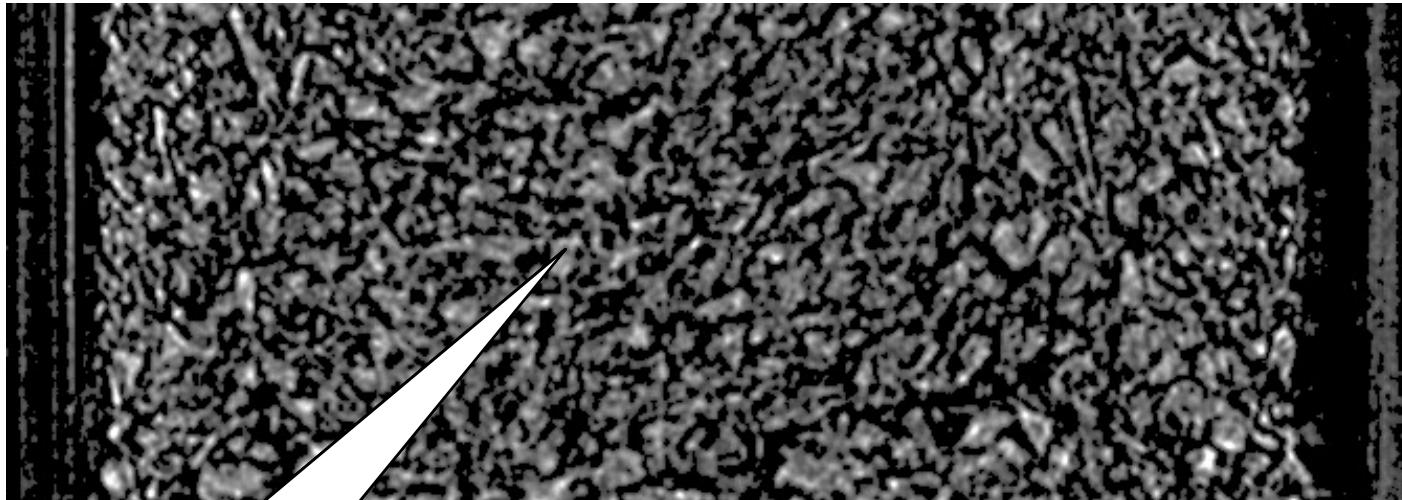
$$\nabla \cdot \mathbf{D}(\mathbf{r}) = \rho(\mathbf{r})$$
$$\nabla \times \mathbf{E}(\mathbf{r}) = i\omega\mu\mathbf{H}(\mathbf{r})$$
$$\nabla \cdot [\mu\mathbf{H}(\mathbf{r})] = 0$$
$$\nabla \times \mathbf{H}(\mathbf{r}) = \mathbf{J}(\mathbf{r}) - i\omega\mathbf{D}(\mathbf{r})$$
$$= -i\omega\varepsilon\mathbf{E}(\mathbf{r})$$

$$n + ik = c(\varepsilon\mu)^{1/2}$$

Sandia National Laboratories
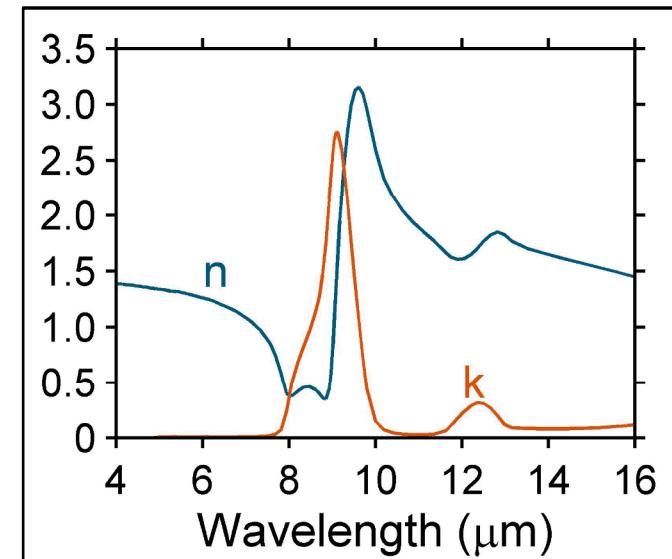
Our Goal, Method, and Focus

- **Goal:** Generate morphologically dependent spectra via physics-based modeling
  - Part of HARD Solids multi-lab project described by Peltz et al. (*Paper 9840-15*)
  - To account for spectral variation as reported by Kulp et al. (*Paper 9840-16*) and Beiswenger et al. (*Paper 9840-17*)

- **Method:** Develop radiative transfer (RT) model w/parametric inputs to be varied in optimizing agreement w/measurements
  - Incorporate fundamental physical properties (*n*,*k*) and account for morphological characteristics with sufficient physical rigor
  - Optimized, the model should demonstrate agreement with reflectance spectra…
 - …while the extracted parameters should agree with independent measurements

- **Focus:** Match model to reflectance spectra of silica powders

Mesh	Size (µm)
325	44
200	74
120	125
100	149
50	297

As presented earlier today by Kulp et al. in *Paper 9840-16*

5

Sandia National Laboratories
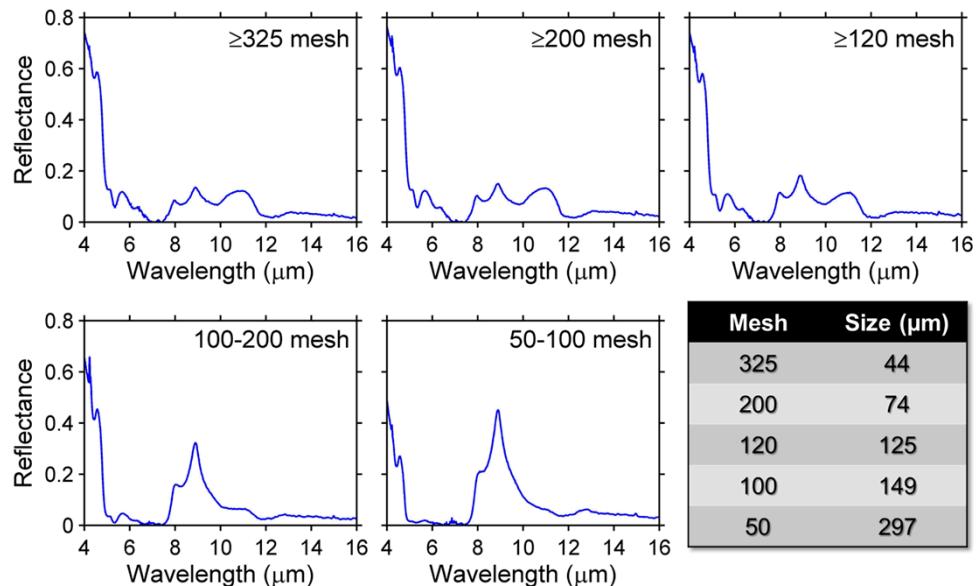
# Invertible Radiative Transfer Model Accounts for Morphological Effects

(1) Forward Model
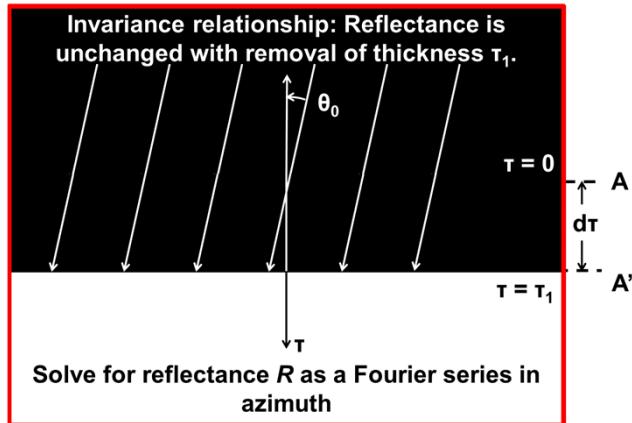


(2) Model Input Parameters

Particle size distribution
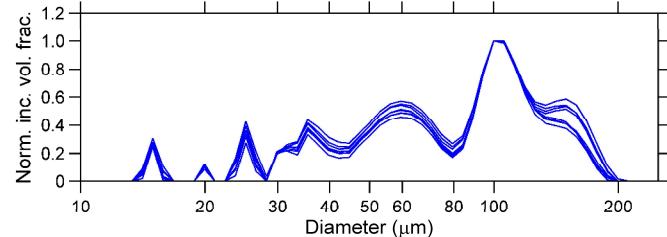
Particle aspect ratios
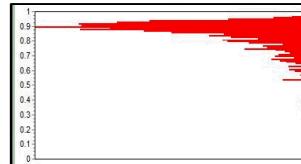
$$\mathbf{x} = x_1, x_2 \ldots x_n$$

(3) Optimizing Model to Data

| Mesh	Size (μm)
325	44
200	74
120	125
100	149
50	297
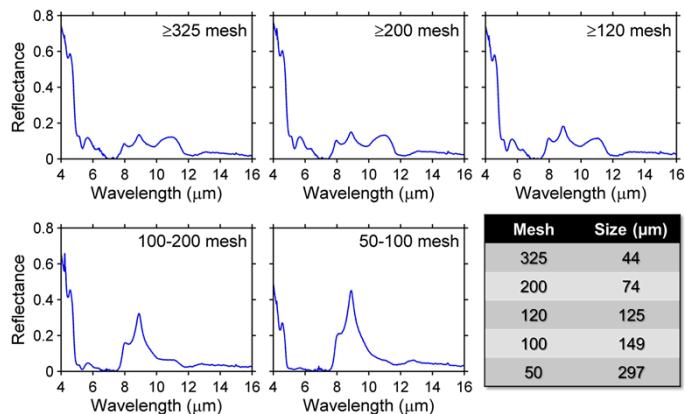
$$f(\mathbf{x}) = \sum_{i=1}^{n} \left| T_i(\mathbf{x}) \right|^2$$

$$\frac{\partial^2 f}{\partial \mathbf{x}^2} = F\left(T_i(\mathbf{x}) \cdot T_i''(\mathbf{x}), \ \left| T_i'(\mathbf{x}) \right|^2 \right)$$

# Plane Albedo (Directional, Hemispherical Reflectance) Measurement
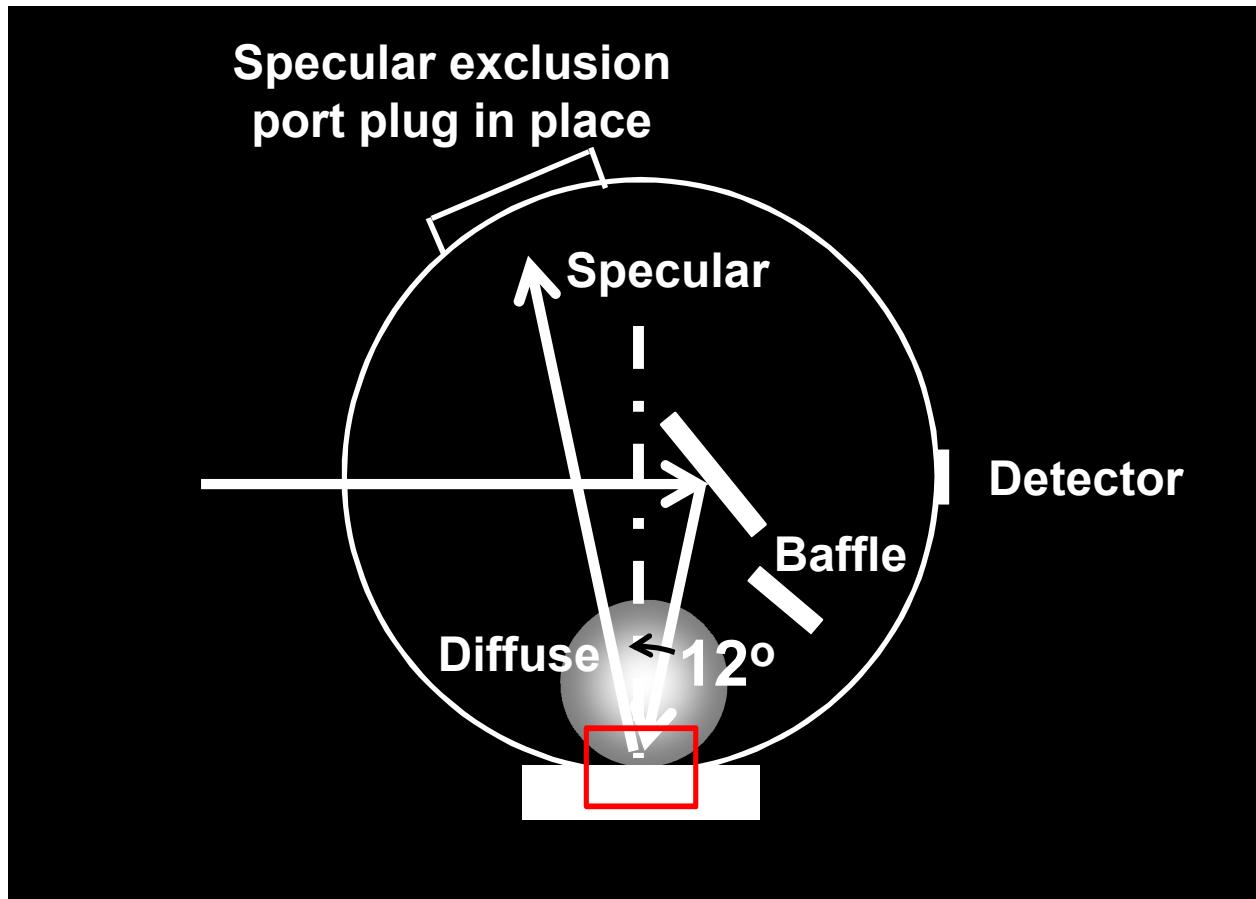


Measuring plane albedo with 12° incidence angle

τ = 0 – – – A

Invariant Imbedding Solution

θ_0

$\tau = 0$

A

θ

$I(\tau,\theta,\phi)$

ϕ

τ

Sandia
National
Laboratories

Invariance relationship: Reflectance is unchanged with removal of thickness τ_1.

θ_0

$\tau = 0$

A

$d\tau$

A'

$\tau = \tau_1$

τ
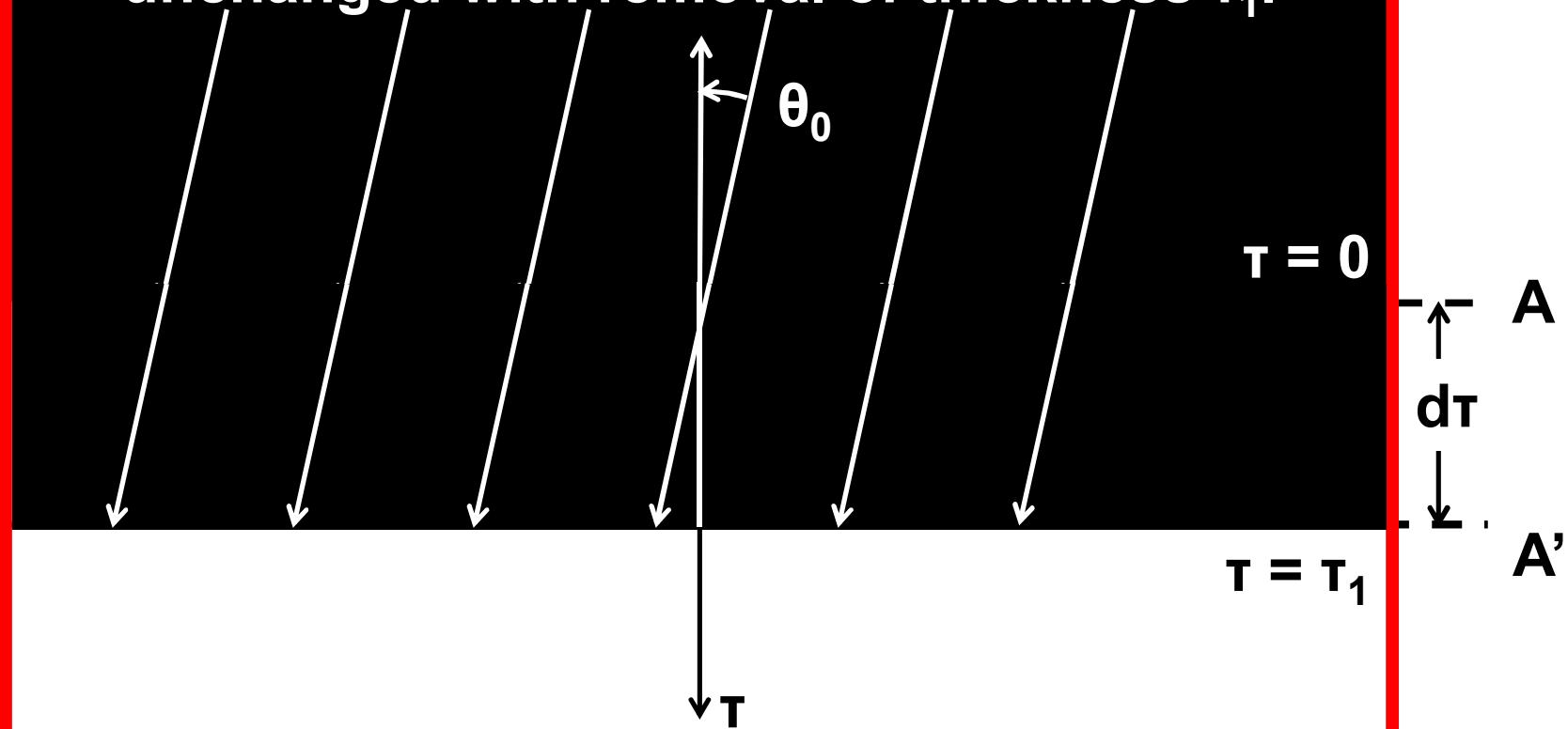
Solve for reflectance R as a Fourier series in azimuth

10

E. G. Yanovitskij, *Light scattering in Inhomogeneous Atmospheres*, Trans. by S. Ginsheimer and O. Yanovitskij, Springer (1997).

$$
\begin{aligned}
(\mu + \mu_0)\, R^m(\mu, \mu_0) =\ & \frac{\varpi}{4} P^m(-\mu, \mu_0) \\
& + \frac{\varpi}{2} \mu_0 \int_0^1 P^m(\mu, \mu')\, R^m(\mu', \mu_0)\, d\mu' \\
& + \frac{\varpi}{2} \mu \int_0^1 R^m(\mu, \mu')\, P^m(\mu', \mu_0)\, d\mu' \\
& + \varpi \mu \mu_0 \int_0^1 \int_0^1 R^m(\mu, \mu')\, P^m(-\mu', \mu'') \\
& \qquad \cdot R^m(\mu'', \mu_0)\, d\mu'\, d\mu''
\end{aligned}
$$

$$P^m, \varpi \longrightarrow R^m$$

Sandia National Laboratories

Solution Provided by Michael Mishchenko (NASA GISS)
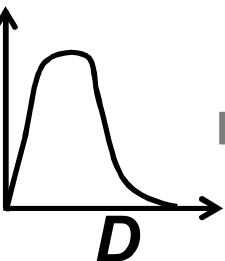
Step #1: n, k ➕ $N(D)$ ➡️ $P^m, \tilde{\omega}$
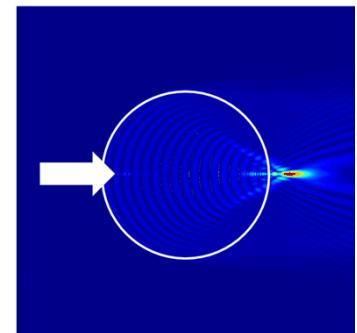
Step #2: $P^m, \tilde{\omega}$ ➡️ R^m

$$(\mu + \mu_0) R^m(\mu, \mu_0) = \frac{\varpi}{4} P^m(-\mu, \mu_0) + \frac{\varpi}{2} \mu_0 \int_0^1 P^m(\mu, \mu') R^m(\mu', \mu_0) \, d\mu'$$

$$+ \frac{\varpi}{2} \mu \int_0^1 R^m(\mu, \mu') P^m(\mu', \mu_0) \, d\mu'$$

$$+ \varpi \mu \mu_0 \int_0^1 \int_0^1 R^m(\mu, \mu') P^m(-\mu', \mu'') \cdot R^m(\mu'', \mu_0) \, d\mu' d\mu''$$

Step #3:
$$\begin{cases} R(\mu, \mu_0, \varphi) = R^0(\mu, \mu_0) + 2 \sum_{m=1}^{m_{\max}} R^m(\mu, \mu_0) \cos(m\varphi) \\ \\ \text{Plane albedo}\,(\mu_0) = \ 2 \int_0^1 R^0(\mu, \mu_0) \mu \ d\mu \end{cases}$$

Sandia National Laboratories

Our Canonical Geometry: Spheroids
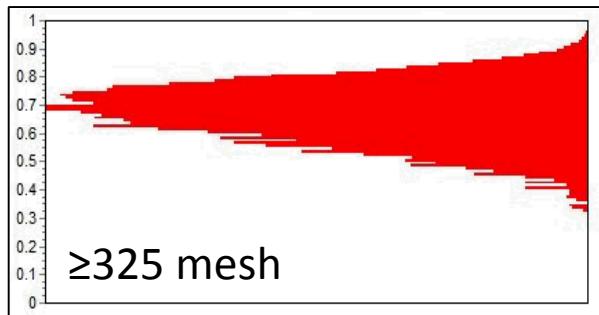
≥325 mesh
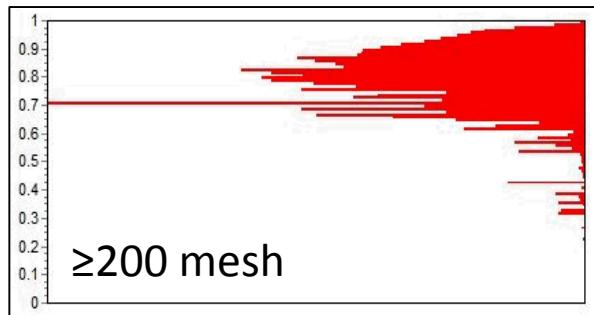
≥200 mesh

≥125 mesh
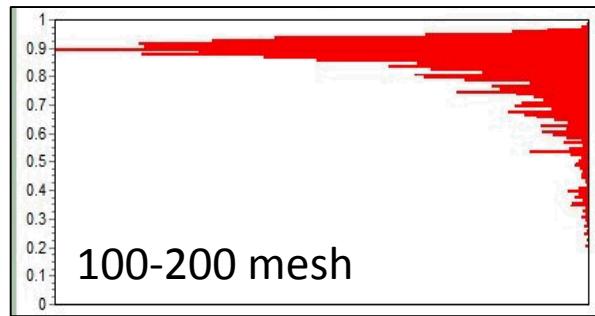
100-200 mesh
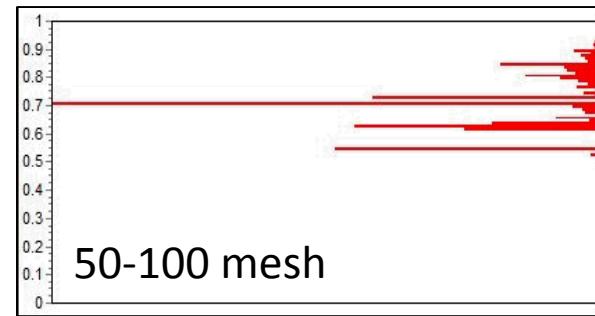
50-100 mesh

- This range of shapes and aspect ratios (ARs) is greatly simplified

- Shape = spheroid, AR = one characteristic value

- 2 shape bins: one bin each per prolate, oblate
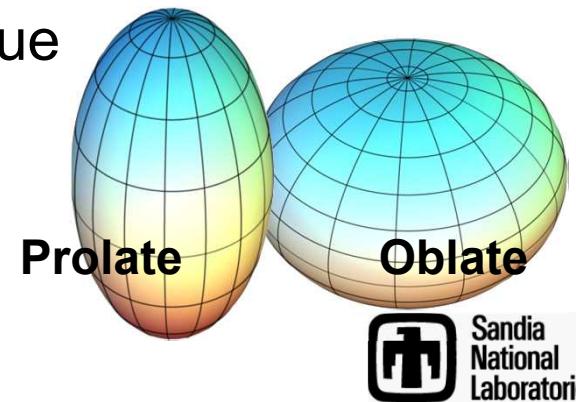
Prolate　　**Oblate**

CAPABILITIES AND LIMITATIONS OF A CURRENT FORTRAN IMPLEMENTATION OF THE *T*-MATRIX METHOD FOR RANDOMLY ORIENTED, ROTATIONALLY SYMMETRIC SCATTERERS

MICHAEL I. MISHCHENKO† and LARRY D. TRAVIS
NASA Goddard Institute for Space Studies, 2880 Broadway, New York, New York 10025, U.S.A.

Abstract—We describe in detail a software implementation of a current version of the *T*-matrix method for computing light scattering by polydisperse, randomly oriented, rotationally symmetric particles. The FORTRAN *T*-matrix codes are publicly available on the World Wide

$$p_{mn} = \sum_{n'=1}^{\infty} \sum_{m'=-n'}^{n'} \left(T_{mnm'n'}^{11} a_{m'n'} + T_{mnm'n'}^{12} b_{m'n'} \right)$$

$$q_{mn} = \sum_{n'=1}^{\infty} \sum_{m'=-n'}^{n'} \left(T_{mnm'n'}^{21} a_{m'n'} + T_{mnm'n'}^{22} b_{m'n'} \right)$$

πD/λ > 120   **+ Diffraction**

procedure convenient in massive computer calculations for particle polydispersions, and Ref. 5 presents benchmark *T*-matrix computations for particles with non-smooth surfaces (finite circular cylinders). A general review of the *T*-matrix method can be found in Ref. 7.

In this paper we provide a detailed description of modern *T*-matrix FORTRAN codes which incorporate all recent developments, are publicly available on the World Wide Web, and are, apparently, the most efficient and powerful tool for accurately computing light scattering by randomly oriented rotationally symmetric particles. For the first time, we collect in one place all necessary formulas, discuss numerical aspects for *T*-matrix computations, describe the input and output parameters, and demonstrate the capabilities and limitations of the codes. The paper is intended to serve as a detailed user guide to a versatile tool suitable for a wide range of practical applications. We specifically target the users who are interested in practical applications of the *T*-matrix method rather than in details of its mathematical formulation.

2. BASIC DEFINITIONS

The single scattering of light by a small-volume element dv consisting of randomly oriented, rotationally symmetric, independently scattering particles is completely described by the ensemble-averaged extinction, C_{ext}, and scattering, C_{sca}, cross sections per particle and the dimensionless

† Author to whom correspondence should be addressed.

309

Applicability of regular particle shapes in light scattering calculations for atmospheric ice particles

Andreas Macke and Michael I. Mishchenko

We ascertain the usefulness of simple ice particle geometries for modeling the intensity distribution of light scattering by atmospheric ice particles. To this end, similarities and differences in light scattering by axis-equivalent, regular and distorted hexagonal cylindric, ellipsoidal, and circular cylindric ice particles are reported. All the results pertain to particles with sizes much larger than a

erably larger than the wavelengths of the incoming solar radiation, especially in the visible spectral region. Therefore, the geometrical optics approximation offers a conceptually simple although time-consuming way to simulate single scattering by almost arbitrarily shaped scatterers.[1–5] Whereas these papers take more and more complex particle geometries such as bullet rosettes, dendrites, or polycrystals into account, in this paper we examine the possibility of representing the scattering proper-

On the other hand, the three (two) semiaxes of an ellipsoid (circular cylinder) allow for a variability of particle shapes that may cover to some extent the natural variability of atmospheric ice crystal habits.

Another motivation arises from uncertainties in our knowledge of real ice particle shapes. The study of observationally derived two-dimensional ice crystal shadow images[6] or replicas[7,8] clearly demonstrates that solid hexagonal columns or plates are a strong idealization of atmospheric ice crystals. However, statistically reliable shape information is difficult to extract from these data, partly because of the strong natural variability. Therefore it appears reasonable to ascertain the use of nonhexagonal but still simple geometries as substitutes for a polydispersion of complicated ice particle shapes.

Because of the lack of sharp edges, ellipsoids do not provide strong halos that are characteristic of regular hexagonal particles. However, the absence of these features, as reported in a number of radiance measurements in or above cirrus clouds,[9,10] emphasizes the potential use of nonhexagonal par-

The authors are with the NASA Goddard Institute for Space Studies, 2880 Broadway, New York, New York 10025. A. Macke is also with the Department of Applied Physics, Columbia University, 2880 Broadway, New York, New York 10025. M. I. Mishchenko is also with the Institute of Terrestrial and Planetary Atmospheres, State University of New York at Stony Brook, Stony Brook, New York 11794.

15

Particle Size Distribution (PSD)
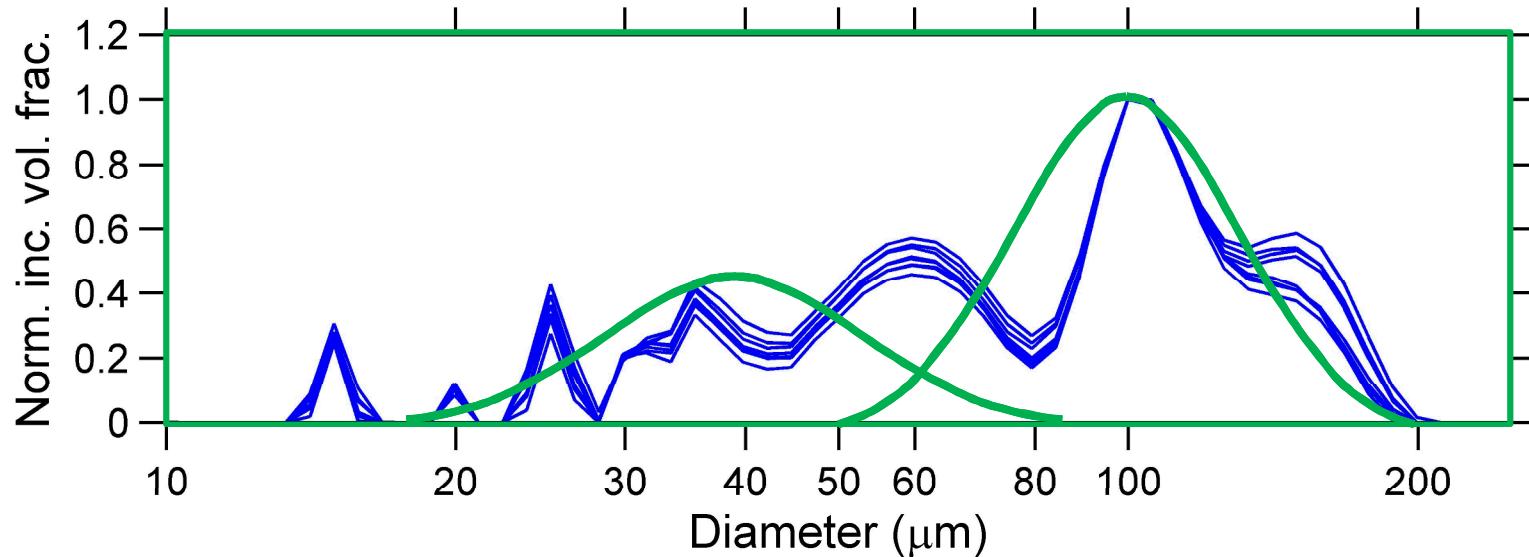
- Approximate with volume *bimodal* log-normal distribution

$$n(r) = \text{constant} \times r^{-4} \left\{ \exp\left[-\frac{(\ln r - \ln r_{g1})^2}{2\ln^2 \sigma_{g1}} \right] + \gamma \cdot \exp\left[-\frac{(\ln r - \ln r_{g2})^2}{2\ln^2 \sigma_{g2}} \right] \right\}$$

- 5 parameters: r_{g1}, σ_{g1}, r_{g2}, σ_{g2}, γ

Sandia National Laboratories

"Patching" the Scattering Properties

- The radiative transfer equation (RTE) is strictly applicable only for sparse media (packing density < 1%)

- **S(θ): Static structure factor (SSF)**
  - Acts as a multiplier to the scattering cross section and phase function
  - Analytical expression available for monodisperse spheres

$$p(\theta) = \frac{4\pi}{C_{sca}} \frac{dC_{sca}}{d\Omega} S(\theta)$$
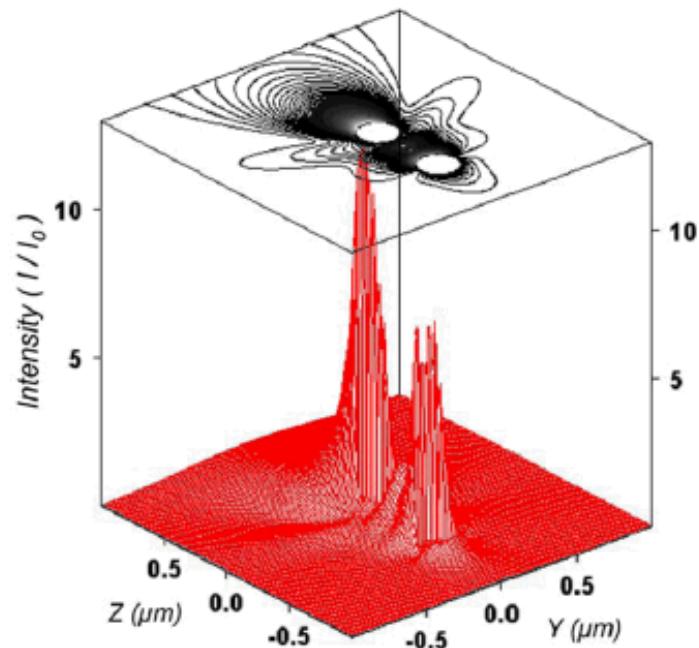
J.-C. Auger and B. Stout, "Local field intensity in aggregates illuminated by diffuse light: T matrix approach," Appl. Opt. **47**, 2897-2905 (2008).

"Patching" the Scattering Properties

- The radiative transfer equation (RTE) is strictly applicable only for sparse media (packing density < 1%)

$$p(\theta) = \frac{4\pi}{C_{\text{sca}}} \frac{dC_{\text{sca}}}{d\Omega} S(\theta)$$

- ***S(θ): Static structure factor (SSF)***
  - Acts as a multiplier to the scattering cross section and phase function
  - Analytical expression available for monodisperse spheres
  - $S(\theta) = F(f_{SSF}, u)$

  - $u = \dfrac{8\pi r_0}{\lambda} \sin\left(\dfrac{\theta}{2}\right)$

  $= 4\left(\dfrac{\pi D}{\lambda}\right) \times \sin\left(\dfrac{\theta}{2}\right)$

Scattering angle
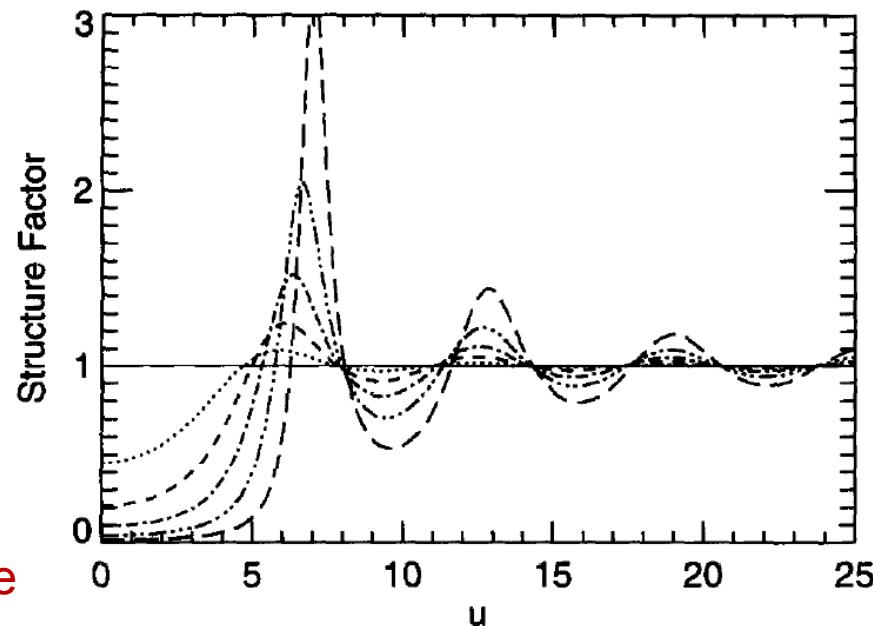
Size parameter

M. I. Mishchenko, "Asymmetry parameters of the phase function for densely packed scattering grains," JQSRT **52**, 95-110 (1994).

18

Surface Roughness

- Range of incidence angles: θ_0 characterized by $\theta_{0,eff}$

- Rougher surface → Larger $\theta_{0,eff}$
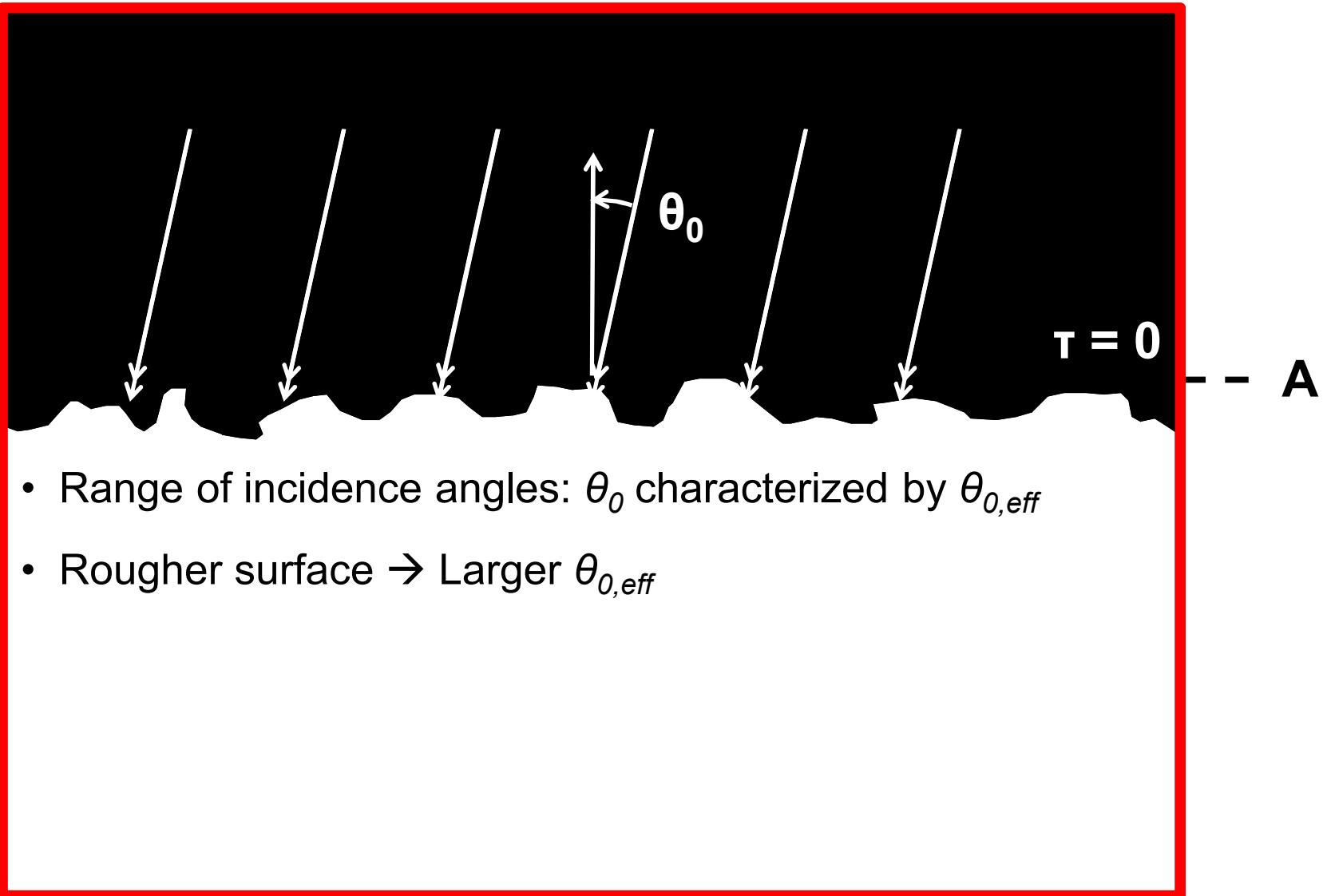
Impact of Packing Density on 1ˢᵗ-Surface Reflection
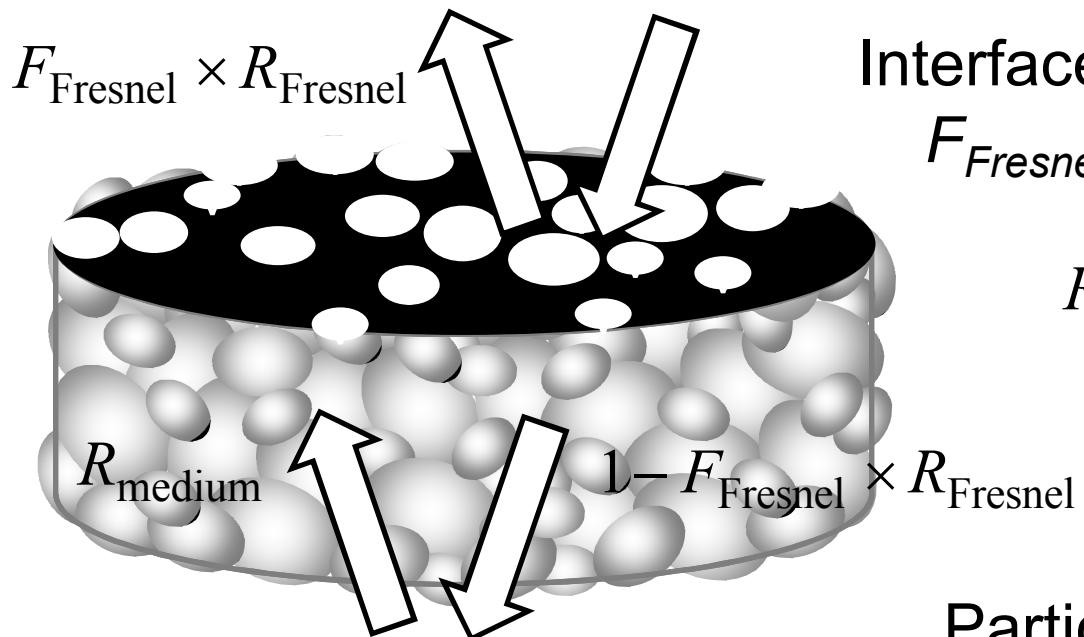
$F_{\mathrm{Fresnel}} \times R_{\mathrm{Fresnel}}$

Interface treated as fractional area $F_{Fresnel}$ of refractive index $n+ik$

$$R_{\mathrm{Fresnel}} = \frac{(n-1)^2 + k^2}{(n+1)^2 + k^2}$$

R_{medium}

$1 - F_{\mathrm{Fresnel}} \times R_{\mathrm{Fresnel}}$

Particulate medium treated as distribution of spheroidal particles of refractive index $n+ik$

$$R = F_{\mathrm{Fresnel}} \times R_{\mathrm{Fresnel}} + \left(1 - F_{\mathrm{Fresnel}} \times R_{\mathrm{Fresnel}}\right) \times R_{\mathrm{medium}}$$

Sandia National Laboratories

Optimizing Model to Measurements

AR

$r_{g1},\ \sigma_{g1},\ r_{g2},\ \sigma_{g2},\ \gamma$

f_{SSF}

$F_{Fresnel}$

$\theta_{0,eff}$

9 parameters

Computational Model

$$(\mu + \mu_0)R^m(\mu, \mu_0)$$

$$= \frac{\varpi}{4}P^m(-\mu, \mu_0)$$

$$+ \frac{\varpi}{2}\mu_0\int_0^1 P^m(\mu, \mu')\,R^m(\mu', \mu_0)\,d\mu'$$

$$+ \frac{\varpi}{2}\mu\int_0^1 R^m(\mu, \mu')\,P^m(\mu', \mu_0)\,d\mu'$$

$$+ \varpi\mu\mu_0\int_0^1\int_0^1 R^m(\mu, \mu')\,P^m(-\mu', \mu'')$$

$$\cdot R^m(\mu'', \mu_0)\,d\mu'\,d\mu''$$

Compare to measured reflectance spectrum

Sandia National Laboratories
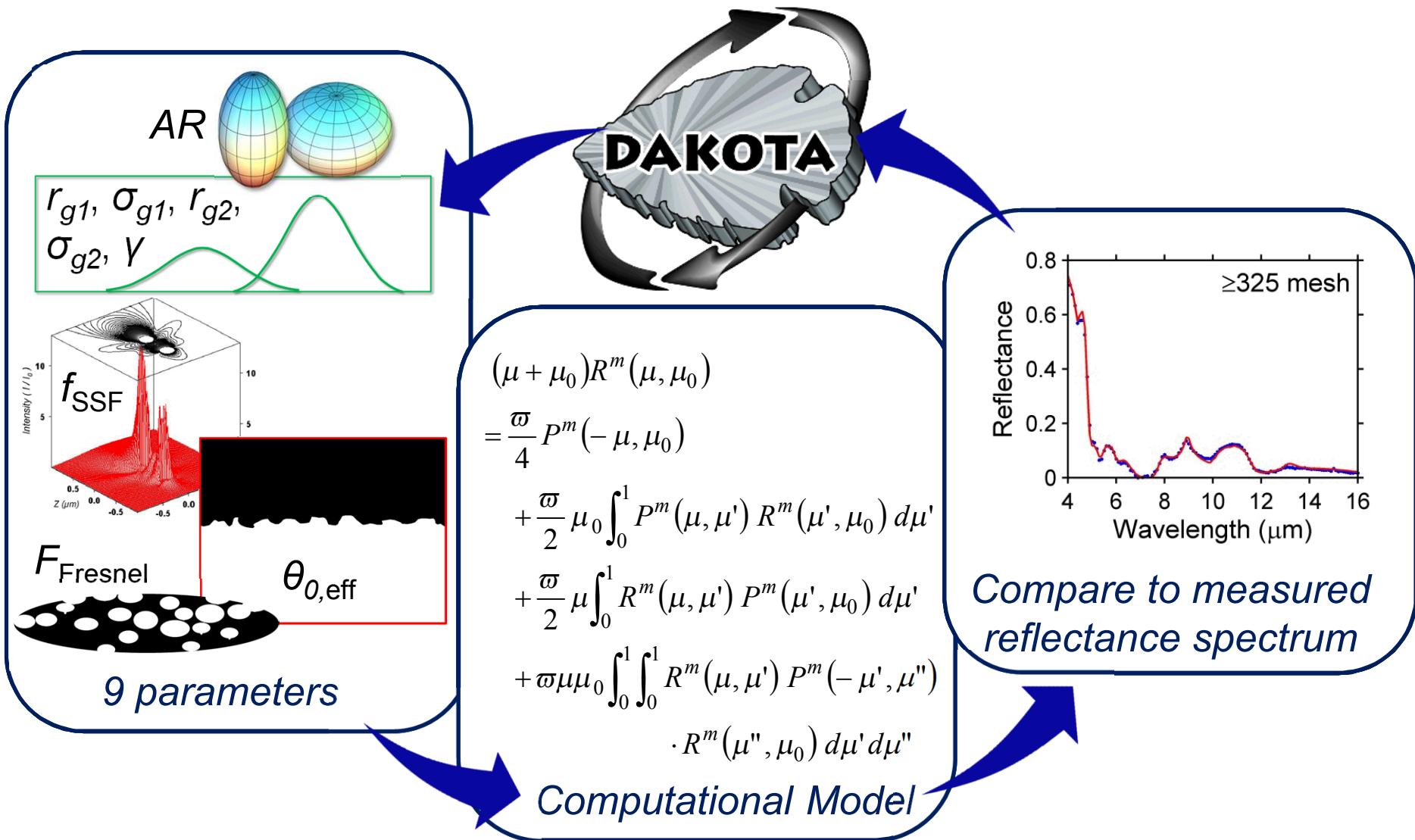
Optimization via "nl2sol" in DAKOTA

- 121 λs: 4-16 µm @ 0.1 µm resolution

- The 121 λ-dependent calculations are divided among 64 processors (4 nodes, 16 cores/node)

- ~10 min/spectrum, 100+ such calculations required for convergence

- The Jacobian (matrix of 1st-order partial derivatives) is numerically determined through forward difference calculations

- The Hessian (matrix of 2nd-order partial derivatives) is numerically approximated from special properties of the sum-of-squares
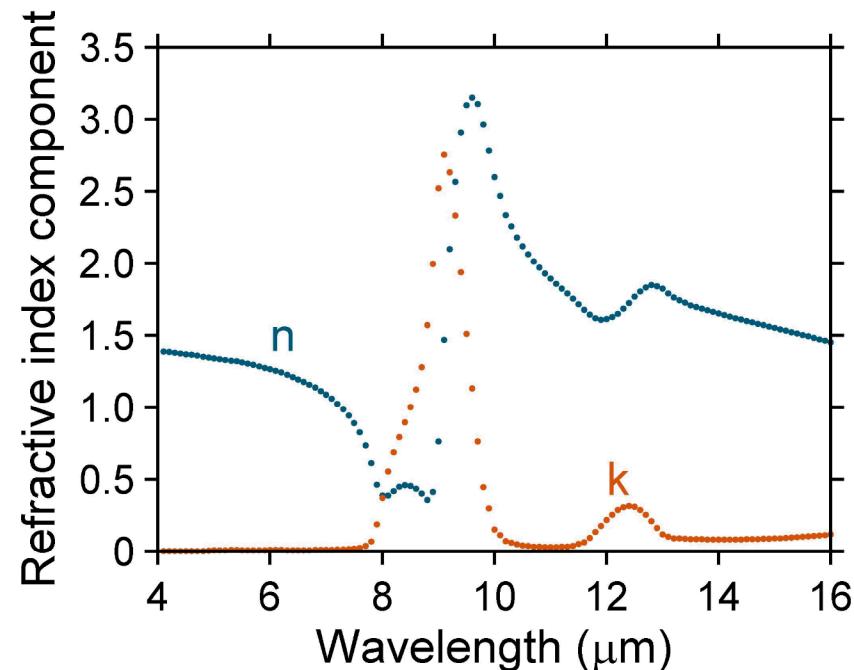
Measured Reflectance Spectra of Silica Powders
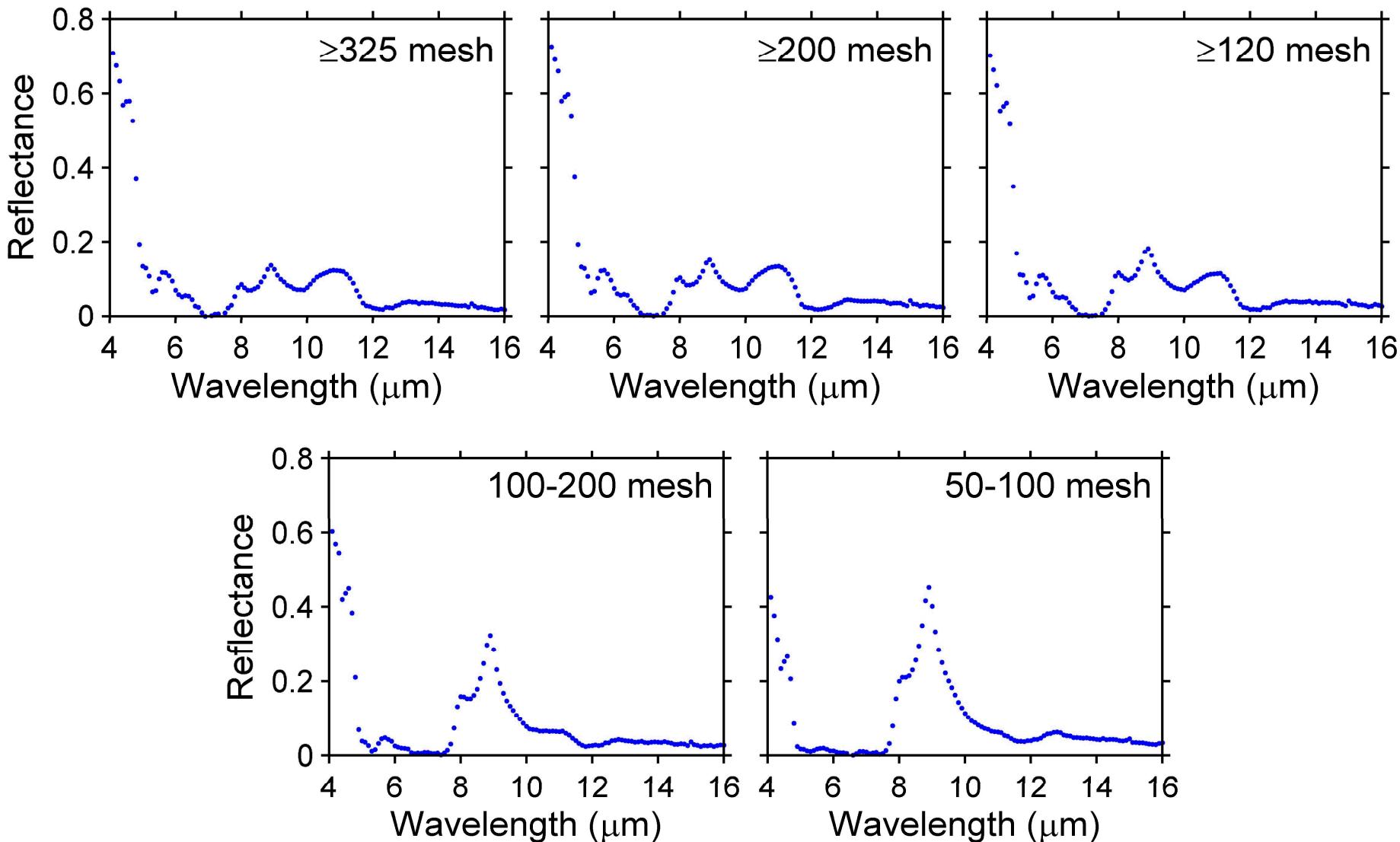
Modeled Reflectance Spectra of Silica Powders
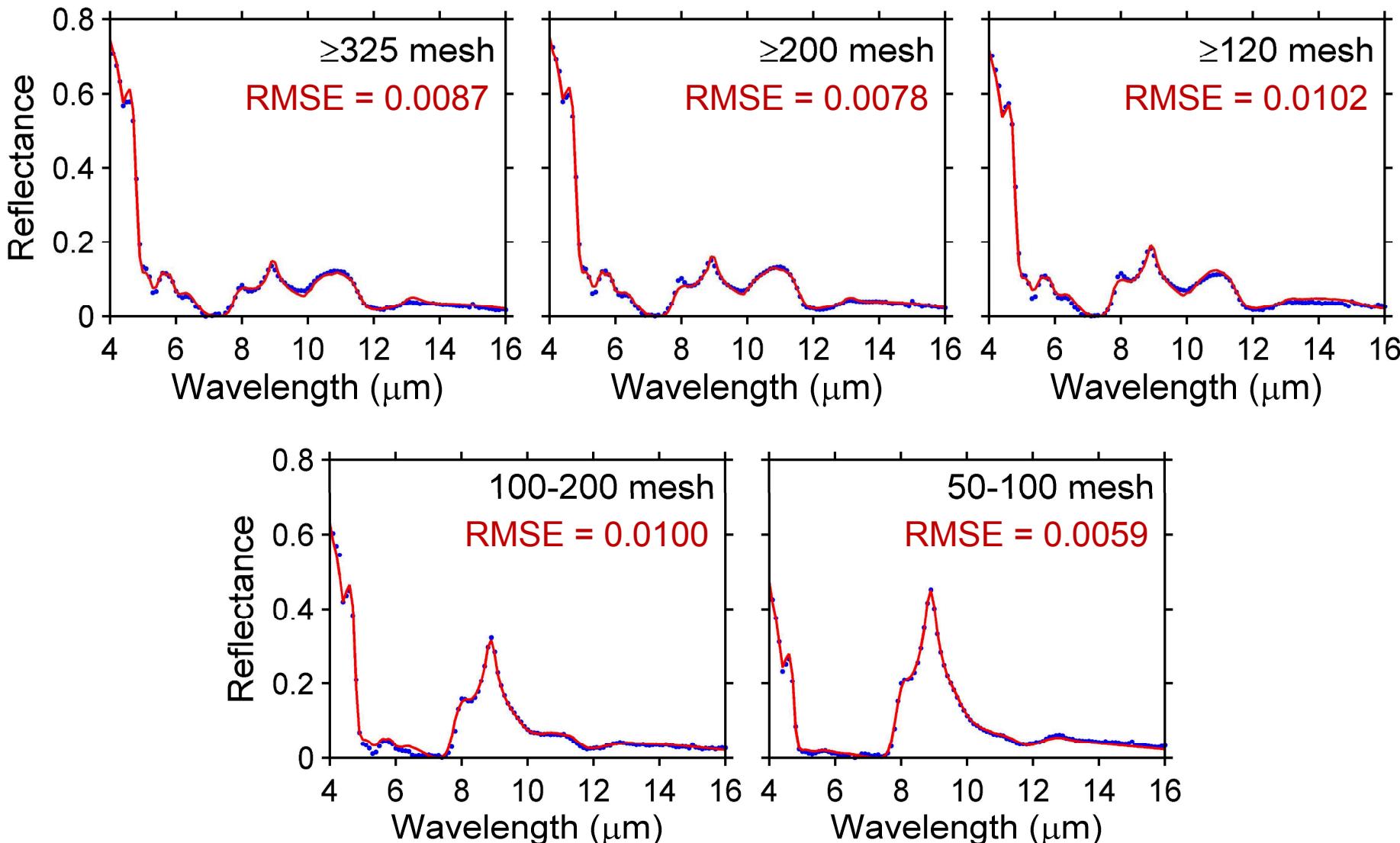
*"Optimized, the model should demonstrate agreement with reflectance spectra … <u>while the extracted parameters should agree with independent measurements</u>"*

So compare model-extracted PSDs w/PSDs measured via laser diffraction
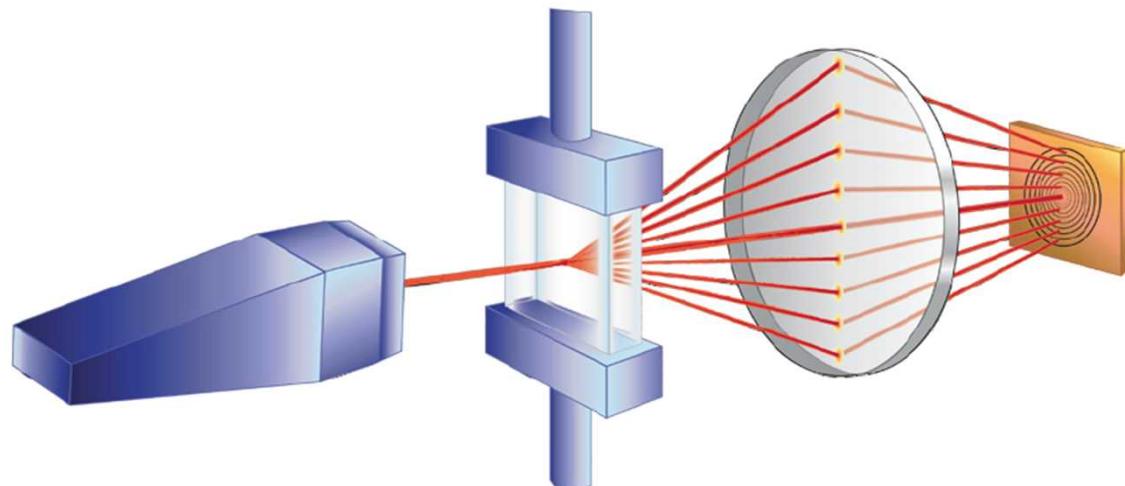
- Visible-light illuminates particles in a flow cell

- Resulting diffraction used to measure PSD

- As presented earlier today by Kulp et al. (Paper 9840-16)

Sandia National Laboratories

Measured PSDs vs Reflectance-Extracted PSDs
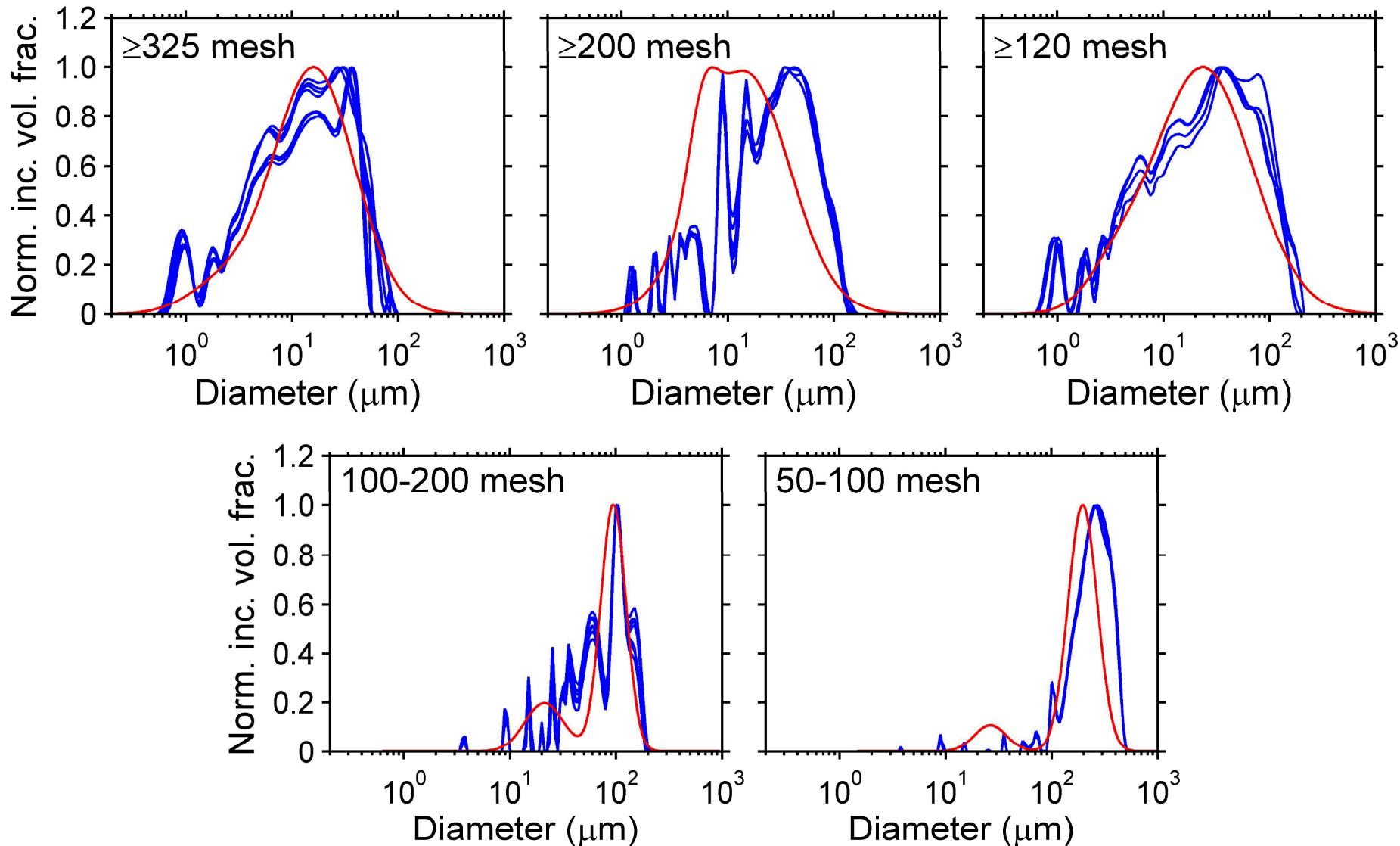
"Generate morphologically dependent spectra via physics-based modeling"

Gravimetrically measured f_{SSF}
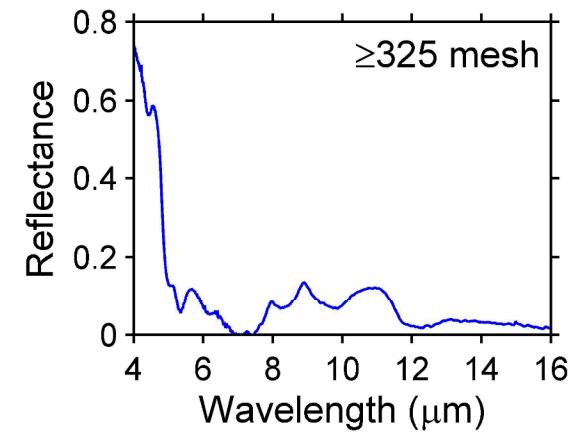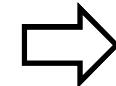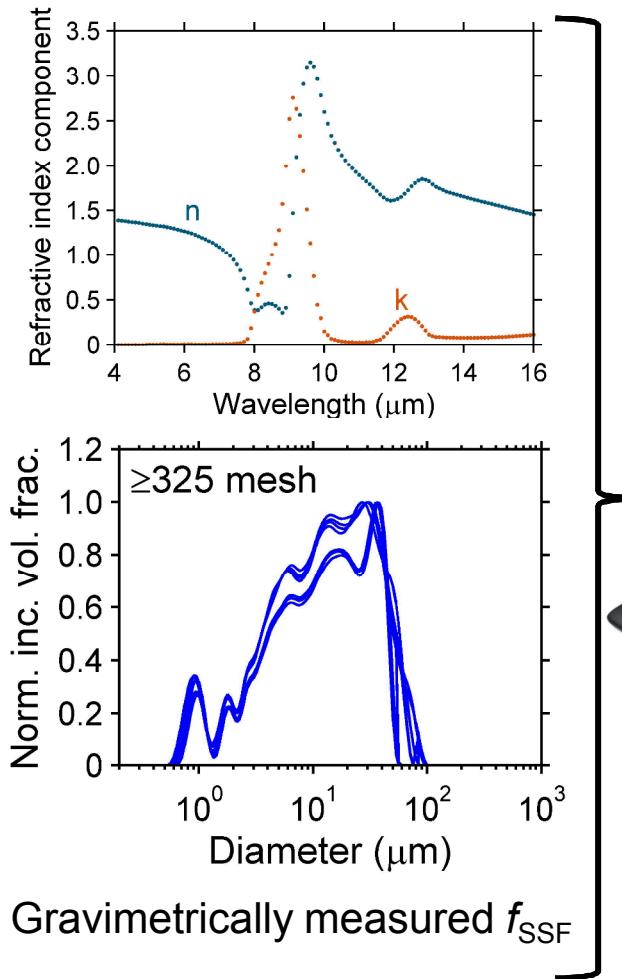
# Modeling Results using Laser-Diffraction PSD and Gravimetric f_{SSF}
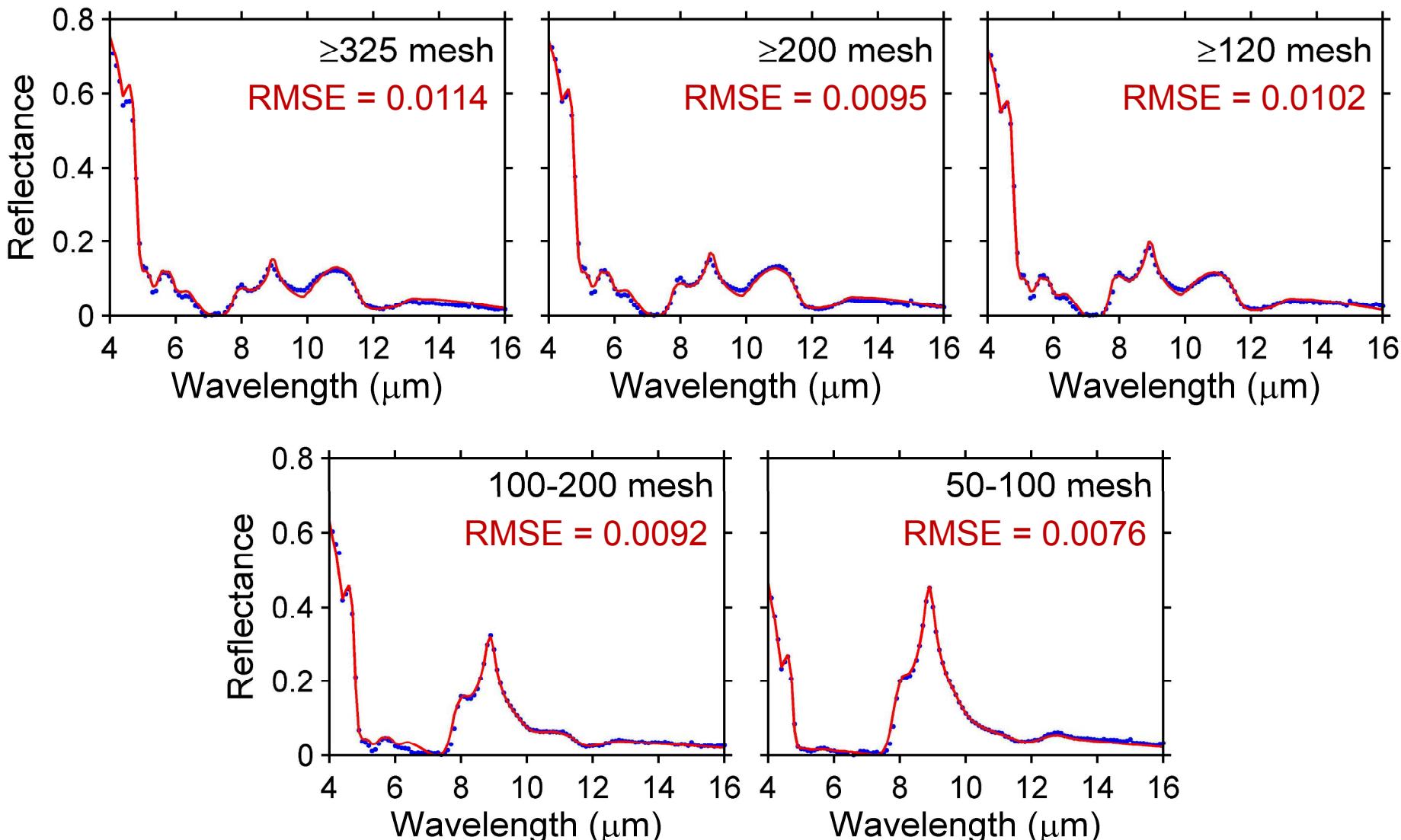
Summary and Conclusions

- Demonstrated physics-based model for the reflectance spectrum of an optically thick particulate surface
  - Requires as input both fundamental optical properties (n,k) and morphological parameters (PSD, packing density, surface roughness)
  - Optimized, the model spectra demonstrate agreement with measured spectra
  - And, with the exception of the ≥200 mesh, the extracted PSDs agree well with laser-diffraction-based measurements
  - Reflectance spectra can be calculated from measured PSDs and fill factors

- Further assessment(s) required
  - Model demonstrated, as of yet, on only one material (silica)
  - Additional materials will be tested as n,k values and ideal-system measurements are available, as presented in earlier today by Kulp et al. (*Paper 9840-16*)
  - Approximation for packing density impact on 1st-surface reflection requires further vetting
  - Ideal-systems of variable packing density being fabricated and measured
  - Model calibration being pursued – to be presented by Engel et al. (*Paper 9840-22*)

Acknowledgments

- Michael Mishchenko (NASA GISS) – Modeling advice and assistance

- Patty Hough (Sandia National Laboratories, CA) – Model inversion via Dakota, parallel computing

- Work supported by the U.S. Department of Energy (DOE) National Nuclear Security Administration (NNSA) Office on Nonproliferation and Verification Research and Development (DNN R&D)

Thanks! Questions?
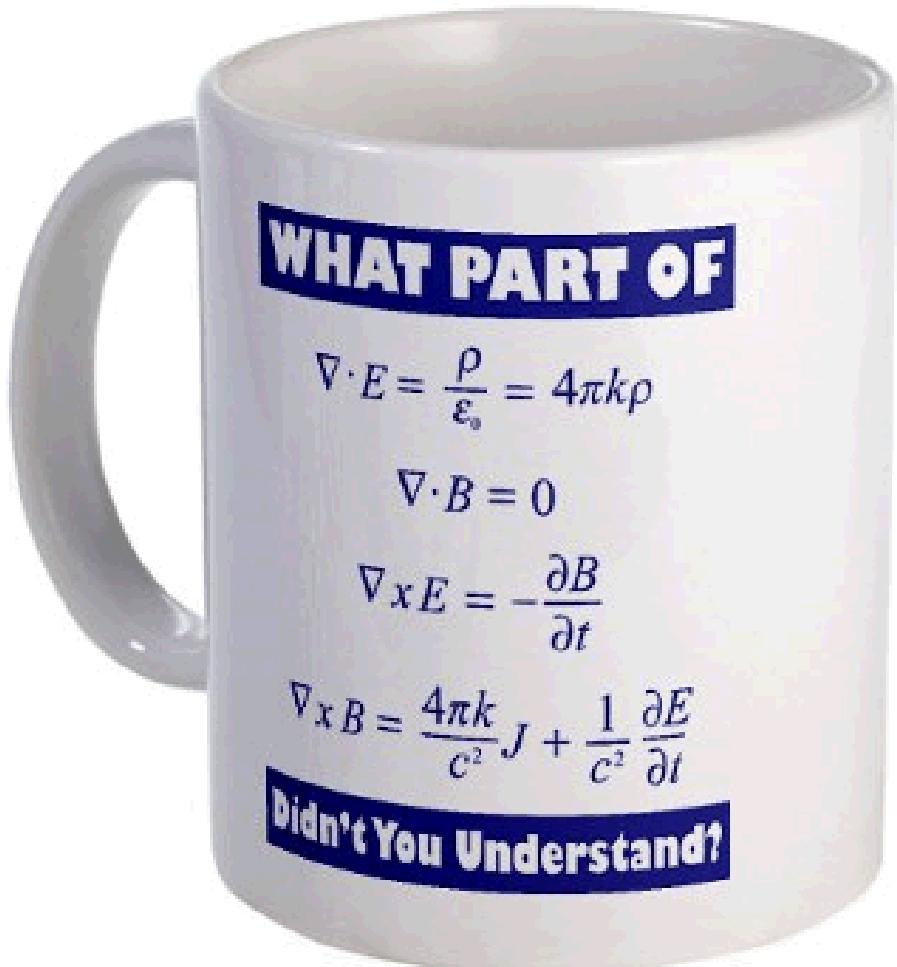
Extra Viewgraphs

Modeling Results using Laser-Diffraction PSD and Gravimetric f_{SSF}

Mesh Range	$\theta_{0,\text{eff}}$	F_{Fresnel}
≥325	0°	0.035
≥200	33°	0.017
≥120	55°	0.035
100-200	57°	0.144
50-100	57°	0.322

Sandia National Laboratories

$$\pi D/\lambda = 120$$
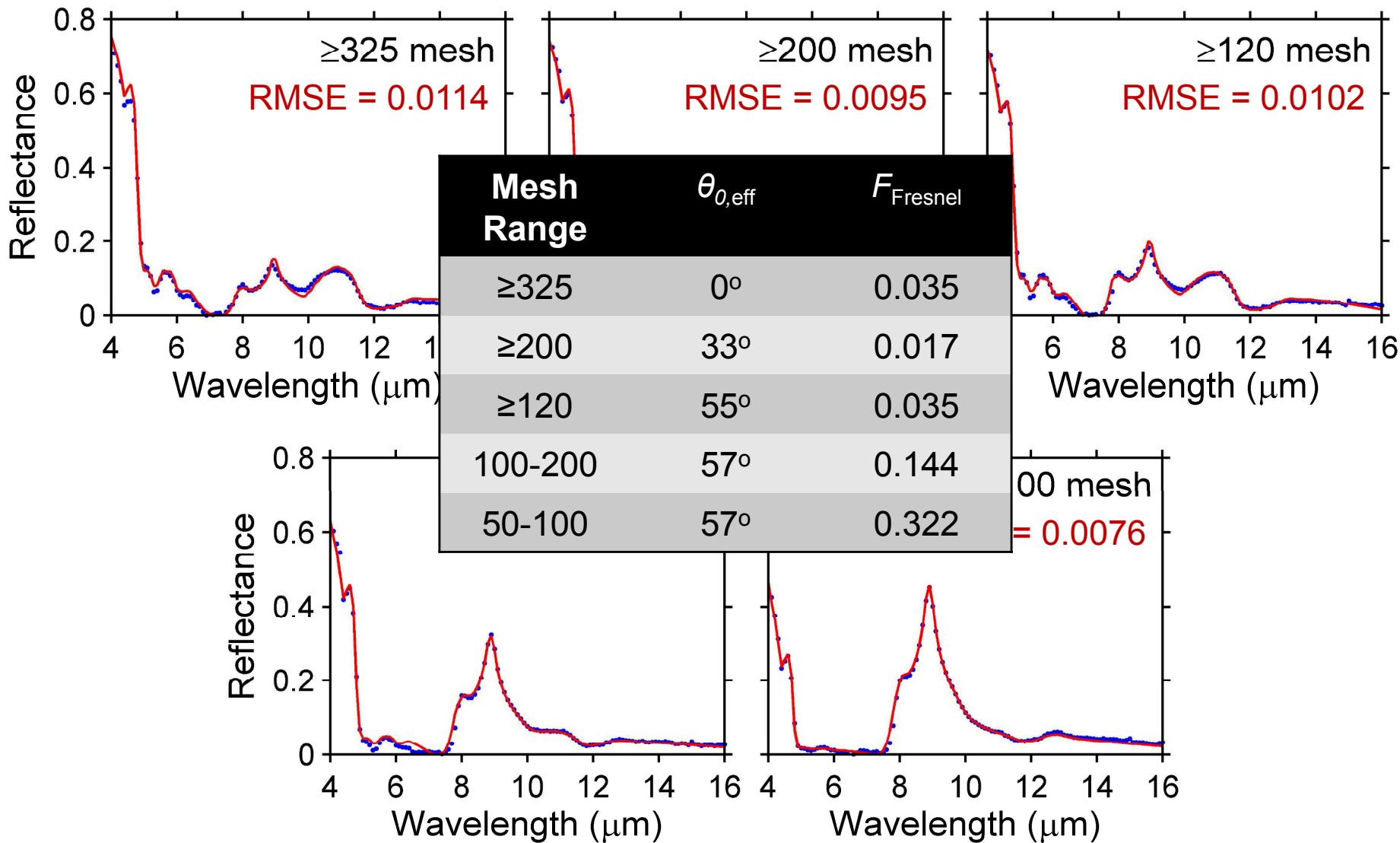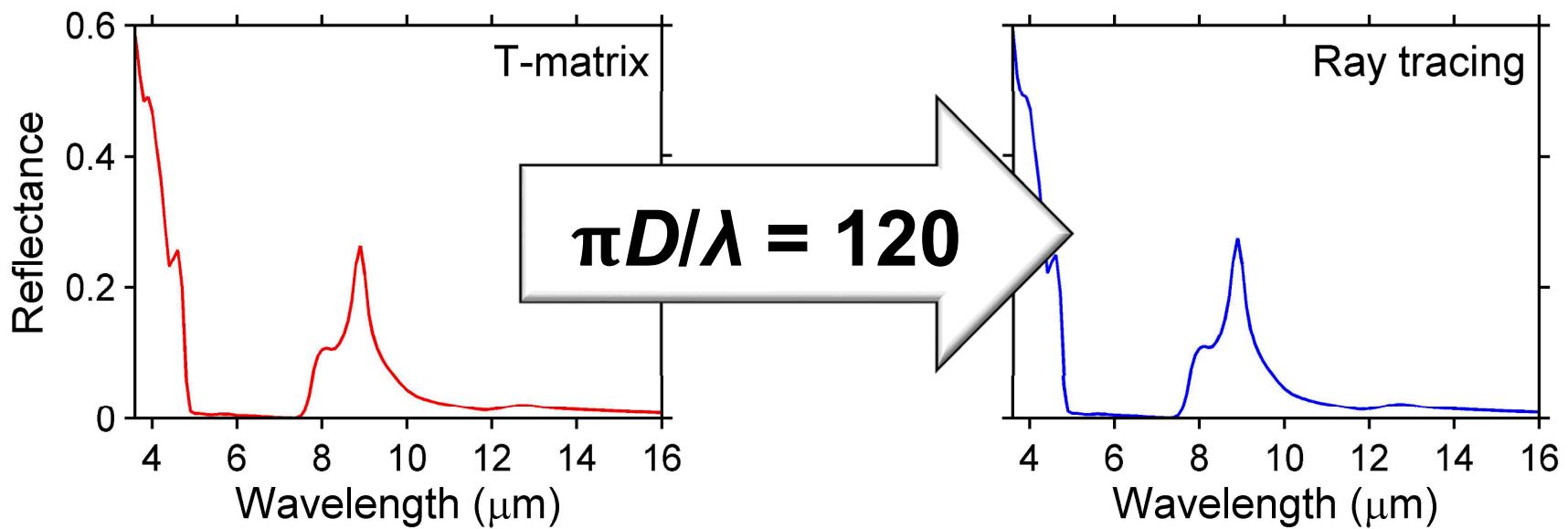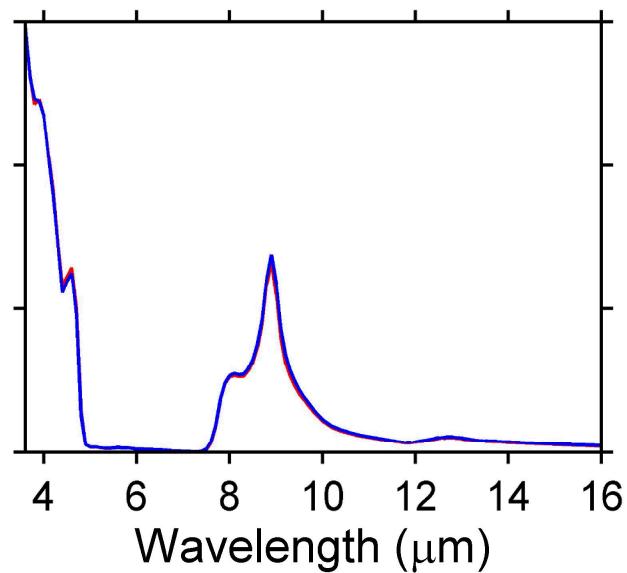
Similar Approximations Made by Others

- J. L. Bandfield, P. O. Hayne, J.-P. Williams, B. T. Greenhagen, and D. A. Paige, "Lunar surface roughness derived from LRO Diviner Radiometer observations," Icarus **248**, 357-372 (2015).

- P. Helfenstein and M. K. Shepard, "Submillimeter-scale topography of the lunar regolith," Icarus **141**, 107-131 (1999).

- M. K. Shepard, R. A. Brackett, and R. E. Arvidson, "Self-affine (fractal) topography: Surface parameterization and radar scattering," J. Geophys. Res. **100**, 11709-11718 (1995).

- B. Hapke, "Bidirectional reflectance spectroscopy. 3. Correction for Macroscopic Roughness," Icarus **59**, 41-59 (1984).

But is this approximation sufficient?

Sandia National Laboratories